Journal of Alloys and Compounds 509 (2011) 7478–7483

Contents lists available at ScienceDirect

Journal of Alloys and Compounds

journal homepage: www.elsevier.com/locate/jallcom

Densification of Al-doped ZnO via preliminary heat treatment under external pressure

Byungjin Hwang[a], Yeong-Kyeun Paek[a], Seung-Ho Yang[b], Sunkwon Lim[b], Won-Seon Seo[c], Kyung-Sik Oh[a,*]

[a] School of Materials Science and Engineering, Center for Green Materials Technology, Andong National University, Andong, Kyungbuk 760-749, Republic of Korea
[b] Heesung Metal Ltd., 693-1, Gojan-Dong, Namdong-Gu, Incheon 405-310, Republic of Korea
[c] Korea Institute of Ceramic Engineering and Technology, 233-5 Gasan, Gumcheon, Seoul 153-801, Republic of Korea

ARTICLE INFO

Article history:
Received 25 October 2010
Received in revised form 15 April 2011
Accepted 15 April 2011
Available online 27 April 2011

Keywords:
Transparent conducting oxide
Al–ZnO
Sintering
Uniformity
External pressure

ABSTRACT

With the doping of Al in ZnO for the preparation of a bulk transparent conductor target, deteriorations were observed in sinterability and uniformity. The doping of 3 wt% Al resulted in the predominance of open pores after sintering at 1300 °C. Less open pores were observed in the ZnO with 2 wt% Al, but the porosity between the inner and outer regions was not uniform due to the preferential evaporation near the surface. To improve both the sinterability and uniformity, mild (<2 MPa) pressure was applied during the preliminary heat treatment at 900 °C, before pressureless final sintering. The pressed specimens showed increased density and uniformity after the final sintering, which were higher than those of the unpressed specimens. The improvements were particularly noticeable in the 3 wt% Al and at 1250 °C, wherein the conventional densification was not successful.

1. Introduction

Various types of electronic devices, such as flat panel displays, solar cells, and touch panels, require transparent conducting electrodes. The transparent conducting material requires 80% optical transmittance and less-than-10^{-3} Ω cm resistivity. As metals should be very thin (3–15 nm) to satisfy such requirements [1,2], indium tin oxide (ITO) is widely used and is also prepared as a target for sputtering. As the stable supply of ITO is threatened, however, by the scarcity of indium, ZnO is being eyed as a strong alternative transparent conducting oxide (TCO). Due to the wide band gap of ZnO of 3.3 eV [3] at room temperature, however, it requires doping [4–7] with trivalent elements such as Al or Ga [6,7] to achieve proper electrical conductivity.

To date, many growth techniques such as magnetron sputtering [8], spray pyrolysis [9], metalorganic chemical vapor deposition [10], and pulsed laser deposition (PLD) [11] have been used to fabricate doped ZnO. Though a target is required for PLD and magnetron sputtering, sufficient information is not available regarding the preparation of the target despite the number of reports [11–27]. One recent report [21] was devoted to the preparation of the target itself, and two reports discussed the effect of the sintering variables such as temperature [27] and atmosphere [14], which provided concrete data and the microstructure of the target. Most of the rest reports [11–13,15–20,22–26] described the preparation of the target merely with a brief sintering condition and the resultant density.

The state of the target is an important issue in the actual manufacturing stage, however, with respect to the prevention of the formation of nodules as well as the prolongation of the target life [28,29]. The nodules are produced with arcing during the sputtering process, and they bring about defective devices [28]. All sources of the uneven distribution of electric charges (e.g., the pores) must be controlled to prevent the formation of nodules. Improved sintering is thus necessary for the preparation of a dense target with a wide range of dopants.

The sintering of indium-based TCO is also a significant issue associated with high vapor pressure [30,31]. Evaporation and condensation at a high vapor pressure coarsen instead of density the particles. Indeed, the density of In_2O_3 decreased with the increase in the sintering temperature from 1400 to 1500 °C [32]. A thermogravimetric analysis [32] also proved the decomposition of In_2O_3 at above 1300 °C. In this respect, volatile materials such as In_2O_3 or ZnO must be sintered at the lowest temperature possible to minimize the densification through volatilization.

Microscopically, sintering extend the grain boundary at the expense of the surfaces of the particles. It also removes the voids among the particles, and shrinks the green body. The shrinkage is

* Corresponding author. Tel.: +82 54 820 5783; fax: +82 54 820 6211.
E-mail address: ksoh@andong.ac.kr (K.-S. Oh).

0925-8388/$ – see front matter © 2011 Elsevier B.V. All rights reserved.
doi:10.1016/j.jallcom.2011.04.085

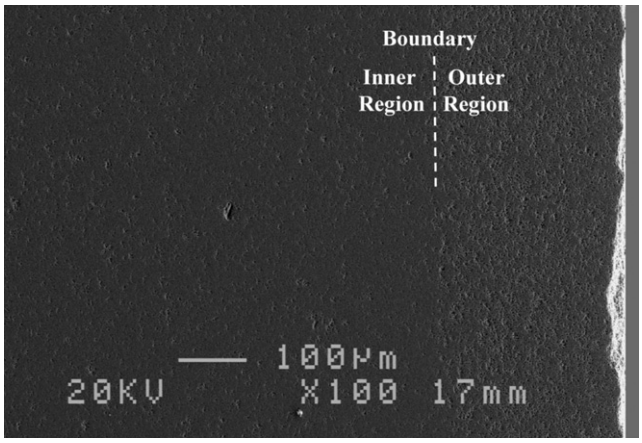

Fig. 1. Typical microstructure of Al doped ZnO that shows the uneven distribution of pores.

not microscopically uniform throughout the green body. At one moment during the initial sintering stage, an agglomerate can exclusively shrink from its surroundings [33]. The local shrinkage induces tensile stress, and the connectivity of the particles around the agglomerates can decrease if the contact is not robust enough across the agglomerate. The local preferential shrinkage leaves a sparse or even void region whose elimination is limited not only because of its size but also because of its energetically stable configuration [34–36]. The presence of stable pores can limit the ultimate densification of the whole specimen [37].

Thus, to improve the sinterability, it is essential to prevent local shrinkage failure and to restore the sintering potential for the final sintering stage. In this study, mild pressure was applied during the preliminary heat treatment before the pressureless final sintering. By applying pressure during the initial sintering stage, the dense packing of the particles was intended to be restored along with the sintering potential. The initial sintering stage was considered the best time for pressing because a proper space for rearrangement can be provided by the maximized difference in the local shrinkage [38]. Such an attempt can allow the specimen to go through the final sintering period with an upgraded sintering potential.

2. Experimental procedures

Al-doped ZnO was prepared from ZnO (Kojundo, 99.99%) and $Al(NO_3)_3{\cdot}9H_2O$ (Showa Chemicals, 98.0%). The $Al(NO_3)_3{\cdot}9H_2O$ was weighed so that the weight percentage of Al (x) would be 1, 2, 3, 4, or 5 in xAl–ZnO after calcination. The $Al(NO_3)_3{\cdot}9H_2O$ was dissolved in distilled water and then mixed with ZnO powder. The mixture was homogenized with 24 h stirring, and then dried in an oven at 100 °C for 48 h. Following heat treatment at 400 °C for 30 min, the powder was ground in an agate mortar and then passed through a 140 mesh (106 μm) sieve.

The prepared xAl–ZnO and pure ZnO powder were placed in a cylindrical mold and pressed at 0.5 MPa for 3 min to yield a green disc. The green body was sealed with rubber and isostatically pressed at 100 MPa for 3 min, using water as the medium. The powder compact was sintered in the air at 900–1350 °C for 2 h, with a heating rate of 5 °C/min. For the heat treatment under pressure, a green compact was placed between two SiC rams in a SiC cylinder. Coarse (5 μm on average) alumina powder was laid around the specimen as a medium for transferring the external pressure from the rams while minimizing the chemical reaction. The mold unit was placed in the furnace that was attached to a materials testing machine (DYMH-100, Daeyeong Co., Korea). The specimen was heated to 900 °C at a rate of 5 °C/min under external pressure (0, 1, or 2 MPa) for 10 min. As soon as the specimen was taken out of the mold after the heat treatment, the coarse alumina powder was removed from the specimen. Then the pressed specimens were sintered at 1250, 1300, or 1350 °C for 2 h in the air using a separate furnace.

The sintered specimens were bisected vertically with a diamond saw for both X-ray diffraction (D/Max 2000, Rigaku Co., Japan) and microstructure analysis. The exposed surface was sequentially polished with SiC abrasive paper and diamond pastes (6, 3, and 1 μm). Then the polished specimens were thermally etched at 1100–1200 °C for 1 h to develop the microstructures. Scanning electron microscopy (JSM-6300, Jeol, Japan) was used at 20 kV for the observation. As some of the specimens were not uniformly porous, as shown in Fig. 1, the inner and outer porosities were separately estimated using the point-counting technique. Considering the thickness of the porous outer region, the outer porosity was estimated within 200 μm from the surface, even in the uniformly porous sample. The average grain size was estimated from the linear intercept length that was determined from the microstructure [39]. The density and porosity of the bulk specimen were also measured, using the Archimedes immersion technique. The relative density of the pure ZnO was calculated by dividing the measured density with the X-ray density of ZnO (5.746 g/ml) [40].

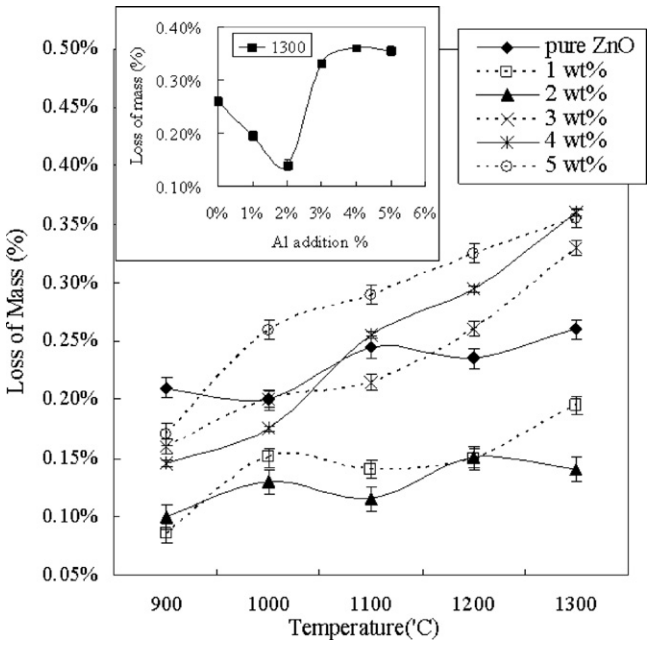

Fig. 2. Losses of mass in xAl–ZnO (x = 0, 1, 2, 3, 4 or 5 wt%) as functions of the sintering temperature and Al addition at 1300 °C (inset).

3. Results and discussion

The loss of mass as a function of the sintering temperature and the amount of Al doping (x) is shown in Fig. 1. For all x, the loss of mass monotonically increased with the temperature. The loss of mass was not monotonic with x, though. In the inserted plot drawn for 1300 °C, the loss of mass initially decreased with x, but was reversed at 2 wt%. Fig. 3 shows the densities with the sintering temperature and x. The green densities before the sintering ranged from 3.17 to 3.19 g/ml without particular dependence on x. The density reached 5.52 g/ml at 900 °C and was saturated with the further increase in the temperature of the pure ZnO. The density at 900 °C corresponded to a 97.2% relative density. The increase in the loss of mass through volatilization is presumed to have balanced the densification that was achieved at the elevated temperature. Unlike with the pure ZnO, the densities obviously increased with the temperature for all the doped ZnOs. As can be seen in the inserted plot that shows the density with x at 1300 °C, the density drastically decreased from 3 wt%. In the 3Al–ZnO that was sintered at 1300 °C, there were 4.3% open pores within the 13.0% total porosity.

On the contrary, the total porosity of 2Al–ZnO was only 3.4% after sintering at 1300 °C without open pores. The drastic increase in the loss of mass of 3Al–ZnO in Fig. 2 began with the appearance of open pores, at which vaporization can take place. From the X-ray diffraction analysis (not shown in this paper), the introduction of 3 wt% Al also induced the precipitation of the spinel phase, known as $ZnAl_2O_4$ [41,42]. The spinel phase is known to suppress the migration of the boundary and to cause deterioration of the sintering properties [43].

The inner (a) and outer (b) porosities with x and the sintering temperature are shown in Fig. 4. In 4Al–ZnO, both the inner and

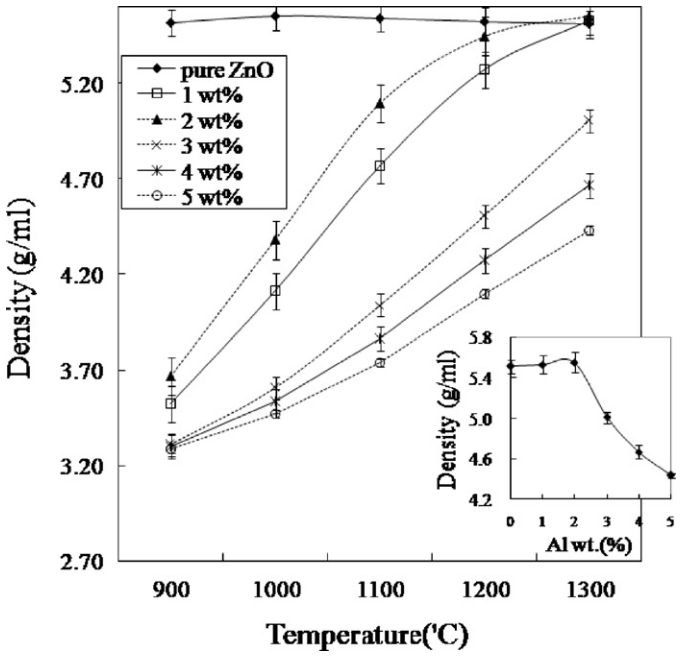

Fig. 3. Densities of *x*Al–ZnO (*x* = 0, 1, 2, 3, 4 or 5 wt%) as functions of the sintering temperature and Al addition at 1300 °C (inset).

outer porosities decreased with the temperature at degrees that were indistinguishable from each other. It should be noted that all the pores were open to the surface, and thus, uniform volatilization should have taken place in the 4Al–ZnO. This trend was also true for 3Al–ZnO, except for the single anomalously small inner porosity at 1100 °C. For the rest of the temperatures, the inner and outer regions were also practically indistinguishable from each other.

For 0 or 1Al–ZnO, the inner and outer regions obviously differed. As shown in Fig. 4, the inner porosities generally decreased with the sintering temperature in the 0 or 1Al–ZnO. On the other hand, the outer porosities for the same *x* first decreased but were reversed at 1200 °C. It should be noted that all the pores were isolated at 1100 °C for the 0 and 1Al–ZnO. Thus, volatilization should have taken place exclusively from the outer region, and should have resulted in an increase in the outer porosity. Therefore, 0 and 1Al–ZnO were regarded as having shown a non-uniform microstructure between their inner and outer regions. It should be noted, however, that the behavior of the 0Al–ZnO differed from that of the doped samples. The pores were scattered in the inner region of 0Al–ZnO. The volume of inner region in 0Al–ZnO was much smaller than those in the doped samples due, for instance, to their sintering at 1100 °C, so the overall porosity was hardly influenced by the inner porosity of the 0Al–ZnO.

In the 2Al–ZnO, the inner and outer porosities varied in the same way as that in the 0 and 1Al–ZnO. As the outer porosity was always greater than the inner porosity, however, each region could be distinguished from the microstructure. Fig. 5 shows the inner and outer microstructures of the 2 and 4Al–ZnO after they were sintered at 1300 °C. The inner and outer regions were indistinguishably porous in the 4Al–ZnO. On the contrary, the inner region was less porous than the outer region in the 2Al–ZnO. Fig. 6 shows the grain sizes of the sintered specimens as a function of the sintering temperature and *x*. Al effectively suppressed the growth of the grains along with the formation of the spinel phase. Consequently, the addition of Al prevented both densification and coarsening.

To promote the densification of the Al-doped ZnO, external pressure (0, 1, or 2 MPa) was applied only during the preliminary heat treatment. Fig. 7 summarizes the densities after the pressureless final sintering at 1250, 1300, and 1350 °C for the Al (*x*) doping variations. Without the application of pressure during the preliminary heat treatment, the density of the specimens averaged from all the *x* values and the final sintering temperature was 5.12 g/ml. The average densities increased to 5.36 and 5.37 g/ml under the external pressure of 1 and 2 MPa, respectively. Therefore, the densities evidently increased with the application of external pressure. The differences between 1 and 2 MPa were not significant on the whole, though. In fact, the densities that were obtained under 1 and 2 MPa were in the same range within an error, so both of them could be termed as 'pressed'. Table 1 summarizes the increases in the densities of the unpressed densities and the improved results from the pressed densities.

Table 1 shows that the increase in the density was very small in the 1Al–ZnO that was sintered at 1300 and 1350 °C. In the 2Al–ZnO, no increase was observed from the sintering at 1350 °C. As 1Al–ZnO can be sintered well even under pressureless conditions, the external pressure had not effect after the sintering at 1300 or 1350 °C. With a relatively poor sintering condition, such as 1250 °C, the external pressure hardly had an effect on the 1Al–ZnO. In the

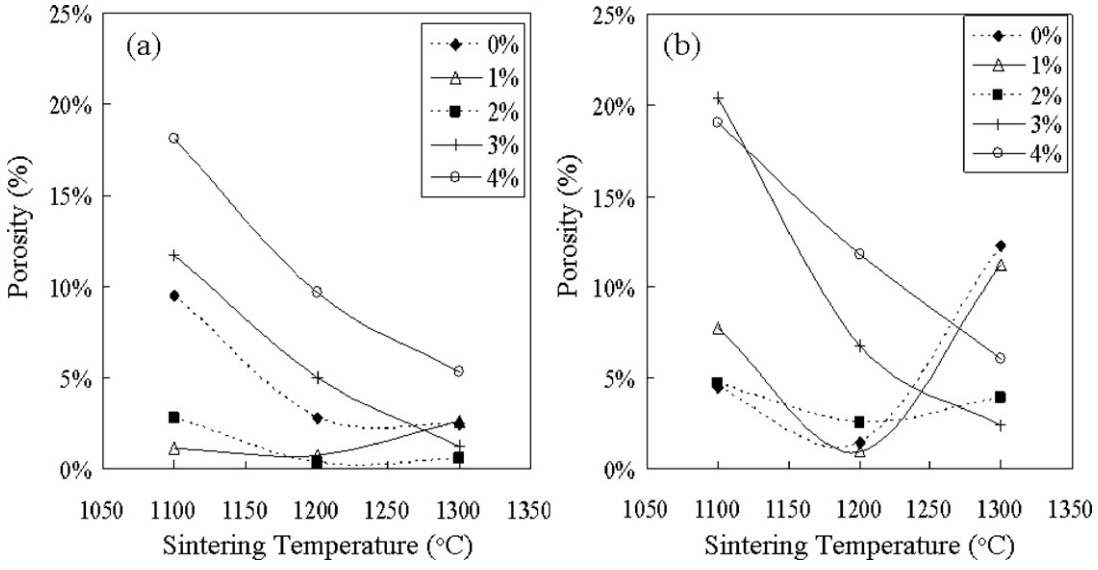

Fig. 4. Inner (a) and outer (b) porosities of *x*Al–ZnO (*x* = 0, 1, 2, 3, or 4 wt%) with the sintering temperature.

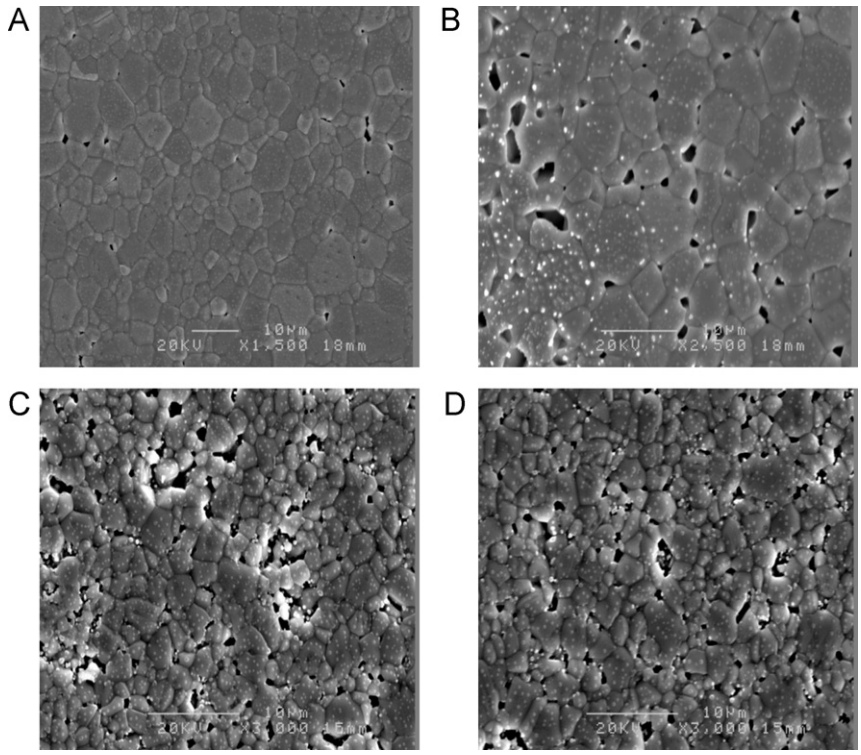

Fig. 5. Microstructures of the *x*Al–ZnO (*x* = 2, or 4 wt%) that was sintered at 1300 °C for 2 h: (A) inner region of *x* = 2; (B) outer region of *x* = 2; (C) inner region of *x* = 4; and (D) outer region of *x* = 4.

case of the 2Al–ZnO, the temperature range at which the external pressure had an effect was expanded to 1300 °C, and a further increase to 1350 °C was observed in the 3Al–ZnO. In the case of the 3Al–ZnO, however, the effect of external pressure on the improvement of the density decreased with the increase in the final sintering temperature. Thus, the improvement of the sinterability via prepressing stood out at a low final sintering temperature and at a high *x*. As *x*Al–ZnO needs to be sintered at the lowest temperature possible, the improvement of the sinterability at a low temperature is beneficial.

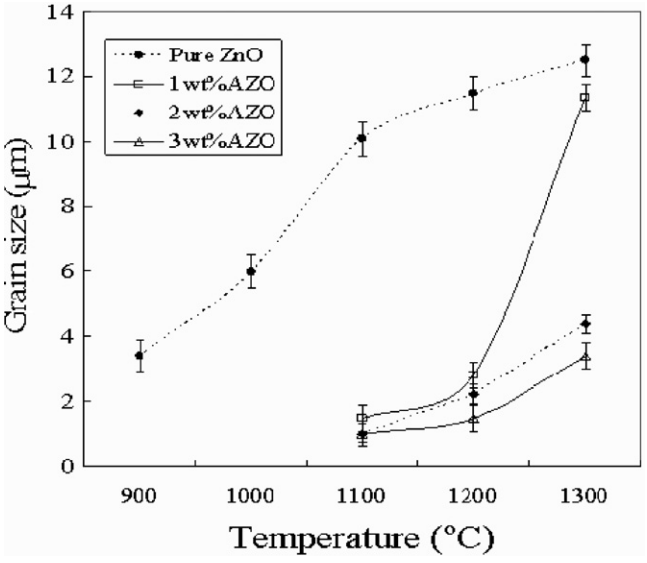

Fig. 6. Grain sizes of *x*Al–ZnO (*x* = 0, 1, 2, or 3 wt%) with respect to the sintering temperature.

The inner and outer microstructures of the 2Al–ZnO that was pressed at 0 or 1 MPa during the preliminary heat treatment are shown in Fig. 8. Without external pressure, the outer region (B) was more porous than the inner region (A). On the contrary, non-

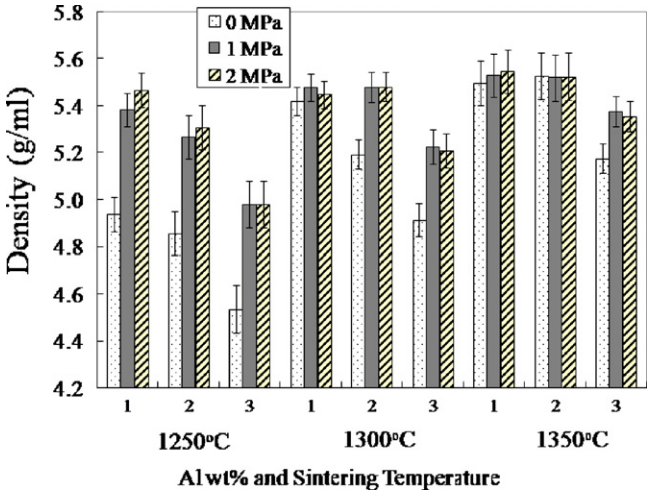

Fig. 7. Densities of the *x*Al–ZnO (*x* = 1, 2 or 3 wt%) that was sintered at 1250, 1300, or 1350 °C with preliminary heat treatment at 900 °C under 0, 1, or 2 MPa pressures.

Table 1
Differences in the densities (g/ml) of the pressed *x*Al–ZnO (*x* = 1, 2 or 3 wt%) and the unpressed *x*Al–ZnO with the final sintering temperatures.

Final sintering temperature (°C)	Doping of Al (wt%)		
	1	2	3
1250	0.53	0.45	0.45
1300	0.06	0.29	0.31
1350	0.05	0.00	0.20

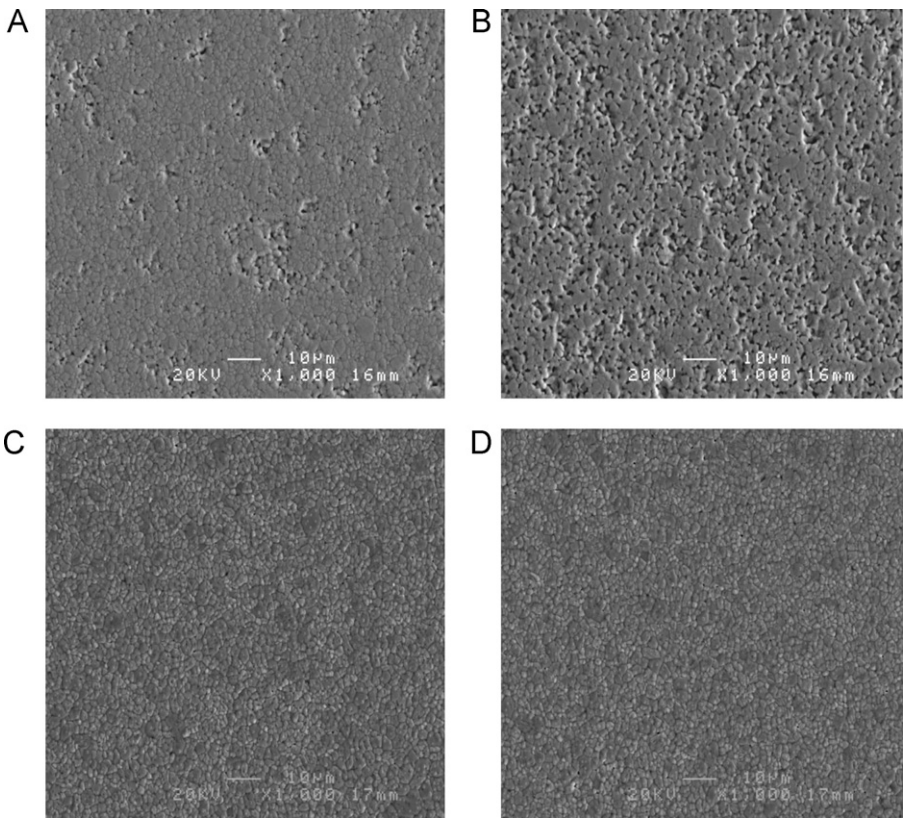

Fig. 8. Microstructures of the 2 wt%Al–ZnO that was finally sintered at 1250 °C for 2 h with previous heat treatment at 900 °C for 10 min under external pressure (0 or 1 MPa): (A) inner region under 0 MPa; (B) outer region under 0 MPa; (C) inner region under 1 MPa; and (D) outer region under 1 MPa.

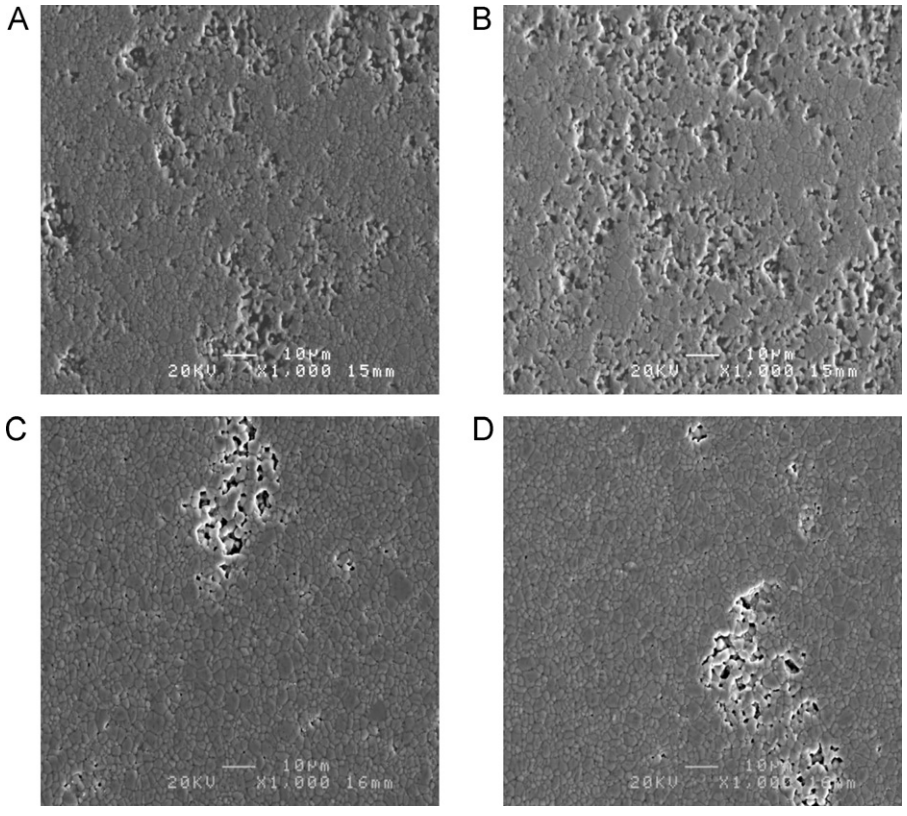

Fig. 9. Microstructures of the 3 wt%Al–ZnO that was finally sintered at 1300 °C for 2 h with previous heat treatment at 900 °C for 10 min under external pressure (0 or 1 MPa): (A) inner region under 0 MPa; (B) outer region under 0 MPa; (C) inner region under 1 MPa; and (D) outer region under 1 MPa.

uniformity was no longer found in the pressed specimen. Both the inner (C) and outer (D) regions were denser than the regions in the unpressed specimen. The early closure of the pores with the aid of external pressure at a moderate sintering temperature (1250 °C) seems to have reduced the evaporation from the surface. Thus, the non-uniform porosity between the inner and outer regions was not noticeable. Fig. 9 shows the microstructures of the inner and outer regions of the 3Al–ZnO. The specimens were sintered at 1300 °C, with previous heat treatment under 0 or 1 MPa. The unpressed specimen was comparatively porous, and the porosities of the inner (A) and outer (B) regions were the same. The application of pressure during the preliminary heat treatment reduced the porosity after the final sintering and maintained the uniform porosity between the inner (C) and outer (D) regions.

An increase in the final density due to pressing during the preliminary heat treatment was also reported for Al_2O_3–ZrO_2 [44] and In_2O_3 [45]. The pressures that were required during the preliminary heat treatment fell within the range of 1–2 MPa [44,45]. Uneven shrinkage of the green body was observed in both the Al_2O_3–ZrO_2 and the In_2O_3. In the case of the Al_2O_3–ZrO_2, the preferential shrinkage of the agglomerate left voids around the agglomerate, which turned into crack-like pores [44] after prolonged sintering. According to the dilatometric analysis of the In_2O_3, the shrinkages peaked at 1070 °C. The shrinkage at 1070 °C was due to the formation of a local dense region called the "domain". It was considered that the pores between the domains were eliminated at 1400 °C, which was expressed as the second maximum peak from the dilatometric shrinkage.

Thus, the preferential shrinkage within the domains at 1070 °C should induce tensile stress around the domains. The tensile stress induced by the domains was estimated as 1–3 MPa, according to Kellet [46]. It is interesting that the magnitude of the induced tensile stress is the same as the pressure required during the preliminary heat treatment. It is thus assumed that the external pressure compensated for the tensile stress that developed during the uneven shrinkage. Microscopically, the applied pressure should reduce the void formed around the domains. The externally applied pressure can be effective if the domains, as matrices, are not too strong, and if there is sufficient space in which to rearrange the domain. Actually, in the case of the In_2O_3, it was most effective to apply pressure just above 1070 °C.

Therefore, pressure must be applied at the very first sintering stage [47]. The pressure that was applied at the final sintering stage in this study was not effective because the matrix was too stiff for the rearrangement of the domains [48]. With the rearrangement of the domains, the sizes of the voids between the domains were reduced. As explained in the driving force for the shrinkage of a void, a smaller void is more advantageous than a larger void for elimination not only because of its size but also because of its driving force. Therefore, the voids that are separated into smaller voids in the preliminary heat treatment have greater driving force for elimination during the final sintering stage, which can elevate the specimen's density.

4. Conclusions

In the sintering of Al-doped ZnO, the increase in Al suppressed the densification and grain growth of ZnO, which implies the reduction of its chemical activity. The loss of mass through volatilization also decreased by up to 2 wt% Al. The further increase in Al from 2 wt%, however, increased the loss of mass due to the appearance of open pores. In the ZnO that was doped with less than 2 wt% Al, the volatilization resulted in non-uniform porosity between the inner and outer regions. To promote the densification of the Al-doped ZnO, mild (1 or 2 MPa) external pressure was applied during the preliminary heat treatment at 900 °C, prior to the final main sintering. Compared to the unpressed specimens, the final density increased to up to 0.53 g/ml after the pressureless final sintering. In particular, the improvement was noticeable in the 3 wt% Al, for which conventional sintering was not effective. It can thus be concluded that the application of external pressure during the preliminary heat treatment is an effective approach for the uniform densification of ZnO for wide Al doping.

Acknowledgements

This work was supported by a Grant-in-Aid for R&D Programs (no. 10030059) from the Korea Ministry of Knowledge Economy.

References

[1] C.P. Liu, Y.T. Hung, Thin Solid Films 492 (2005) 269–274.
[2] N. Benramadane, W.A. Murad, R.H. Misho, M. Ziane, Z. Kebbab, Mater. Chem. Phys. 48 (1997) 119–123.
[3] K. Tominaga, H. Manabe, N. Umezu, I. Mori, Y. Ushiro, I. Nakabayashi, J. Vac. Sci. Technol. A 159 (1997) 1074–1079.
[4] C.P. Liu, G.R. Jeng, H.E. Huang, Mater. Trans. 48 (2007) 847–853.
[5] T. Minami, T. Yamamoto, T. Miyata, Thin Solid Films 366 (2000) 63–68.
[6] A.E. Jimenez-Gonzalez, J. Solid State. Chem. 128 (1997) 176–180.
[7] M. Ohyama, H. Kozuka, T. Yoko, Thin Solid Films 306 (1997) 78–85.
[8] R. Wen, L. Wang, X. Wang, G.H. Yue, Y. Chen, D.L. Peng, J. Alloys Compd. 508 (2010) 370–374.
[9] E. Nishimura, Jpn. J. Appl. Phys. 35 (1996) 2788–2793.
[10] K. Tominaga, T. Murayama, N. Umezu, I. Mori, T. Ushiro, T. Moriga, K. Nakabayashi, Thin Solid Films 343–344 (1999) 160–163.
[11] K. Matsubara, P. Fons, K. Iwata, A.Y. Amada, S. Niki, Thin Solid Films 422 (2002) 176–179.
[12] E.J. Yun, J.W. Jung, B.C. Lee, J. Alloys Compd. 496 (2010) 543–547.
[13] Y. Liu, Q. Li, H. Shao, J. Alloys Compd. 485 (2009) 529–531.
[14] H.S. Huang, H.C. Tung, C.H. Chiu, I.T. Hong, R.Z. Chen, J.T. Chang, H.K. Lin, Thin Solid Films 518 (2010) 6071–6075.
[15] Y.R. Park, E.K. Kim, D. Jung, T.S. Park, Y.S. Kim, Appl. Surf. Sci. 254 (2008) 2250–2254.
[16] E. Nam, Y.H. Kang, D. Jung, Y.S. Kim, Thin Solid Films 518 (2010) 6245–6248.
[17] W.J. Jeong, S.K. Kim, G.C. Park, Thin Solid Films 506–507 (2006) 180–183.
[18] W.J. Jeong, G.C. Park, Sol. Energy Mater. Sol. Cells 65 (2001) 37–45.
[19] J. Oda, J. Nomoto, T. Miyata, T. Minami, Thin Solid Films 518 (2010) 2984–2987.
[20] W. Lin, R. Ma, W. Shao, B. Liu, Appl. Surf. Sci. 253 (2007) 5179–5183.
[21] J. Zhang, W. Zhang, E. Zhao, H.J. Jacques, Mater. Sci. Semicond. Process. (2011), doi:10.1016/j.mssp.2011.02.004.
[22] M. Jiang, X. Liu, Appl. Surf. Sci. 255 (2008) 3175–3178.
[23] H. Koa, W.P. Tai, K.C. Kim, S.H. Kim, S.J. Suh, Y.S. Kim, J. Cryst. Growth 277 (2005) 352–358.
[24] K.P. Bhuvana, J. Elanchezhiyan, N. Gopalakrishnan, T. Balasubramanian, J. Alloys Compd. 473 (2009) 534–537.
[25] H.C. Lu, J.L. Lu, C.Y. Lai, G.M. Wu, Physica B 404 (2009) 4846–4849.
[26] T. Minami, S. Ida, T. Miyata, Y. Minamino, Thin Solid Films 445 (2003) 268–273.
[27] C.P. Liu, G.R. Jeng, J. Alloys Compd. 468 (2009) 343–349.
[28] B.L. Gehman, S. Jonsson, T. Rudolph, M. Scherer, M. Weigert, R. Werner, Thin Solid Films 220 (1992) 333–336.
[29] N. Nadaud, M. Nanot, P. Boch, J. Am. Ceram. Soc. 77 (1994) 843–846.
[30] J.H.W. de Wit, J. Solid State Chem. 13 (1973) 142–149.
[31] T. Vojnovich, R.J. Bratton, Am. Ceram. Soc. Bull. 54 (1975) 216–217.
[32] N. Nadaud, D.Y. Kim, P. Boch, J. Am. Ceram. Soc. 80 (1997) 1208–1212.
[33] F.F. Lange, J. Am. Ceram. Soc. 66 (1983) 396–398.
[34] L.C. DeJonghe, M.L. Rahaman, J. Am. Ceram. Soc. 67 (1984) C214–C215.
[35] W.D. Kingery, B. Francois, Sintering and Related Phenomena, Gordon and Breach, New York, 1967, pp. 471–488.
[36] S.T. Lin, R.M. German, J. Am. Ceram. Soc. 71 (1988) C432–C433.
[37] F.F. Lange, B.I. Davis, I.A. Aksay, J. Am. Ceram. Soc. 66 (1983) 407–408.
[38] C.A. Bruch, Am. Ceram. Soc. Bull. 41 (1962) 799–806.
[39] H.E. Exner, H.L. Lukas, Metallography 4 (1971) 325–338.
[40] R.N. Blumenthal, D.H. Whitmore, J. Electrochem. Soc. 110 (1963) 92–93.
[41] J.P. Wiff, Y. Kinemuchi, H. Kang, C. Ito, K. Watari, J. Eur. Ceram. Soc. 29 (2009) 1413–1418.
[42] W. Komatsu, M. Miyamoto, S. Hujita, Y. Moriyoshi, J. Ceram. Soc. Jpn. 18 (1968) 7–13.
[43] M. Matsuoka, Jpn. J. Appl. Phys. 10 (1971) 736–746.
[44] K.S. Oh, D.Y. Kim, S.J. Cho, J. Am. Ceram. Soc. 79 (1996) 1723–1725.
[45] J.W. Son, D.Y. Kim, P. Boch, J. Am. Ceram. Soc. 81 (1998) 2489–2492.
[46] B.J. Kellet, F.F. Lange, J. Am. Ceram. Soc. 7 (1984) 369–371.
[47] R.K. Bordia, R. Raj, Adv. Ceram. Mater. 3 (1988) 122–126.
[48] K.S. Oh, D.Y. Kim, S.J. Cho, J. Am. Ceram. Soc. 78 (1995) 2537–2540.